

# The effect of a carbon-nanotube forest-mat strike face on the ballistic-protection performance of E-glass reinforced poly-vinyl-ester-epoxy composite armour

M Grujicic<sup>1\*</sup>, W C Bell<sup>1</sup>, S B Biggers<sup>1</sup>, K L Koudela<sup>2</sup>, J F Tarter<sup>2</sup>, and B A Cheeseman<sup>3</sup>

<sup>1</sup>Department of Mechanical Engineering, Clemson University, Clemson, South Carolina, USA

<sup>2</sup>Applied Research Laboratory, Pennsylvania State University, University Park, Pennsylvania, USA

<sup>3</sup>Army Research Laboratory – Survivability Materials Branch, Aberdeen, Maryland, USA

*The manuscript was received on 2 December 2006 and was accepted after revision for publication on 13 August 2007.*

DOI: 10.1243/14644207JMDA136

**Abstract:** In the present work, a ballistic material-model development approach is combined with transient non-linear dynamics simulations of the projectile/armour interactions to explore the armour-hard-facing potential of multi-walled carbon nanotube (MWCNT) reinforced, poly-vinyl-ester-epoxy (PVEE)-matrix composite mats. This approach is applied to improving the ballistic-protection performance of E-glass fibre-mat reinforced PVEE-matrix laminate armour. Two different architectures of the MWCNT-reinforced/PVEE-matrix composite mats were considered: (a) a MWCNT-ply mat structure in which the MWCNT reinforcements are aligned parallel to the armour faces and (b) a MWCNT-forest mat structure in which the MWCNT reinforcements are aligned orthogonally to the armour faces. The projectile/armour interaction simulation results showed that, at low volume fractions of MWCNTs, both armour architectures yield no discernable increase in the armour ballistic-protection performance as measured by the armour. On the other hand, at high MWCNT volume fractions of MWCNTs, the first armour architecture remained ineffective whereas the second showed a minor improvement in the ballistic-protection performance relative to the corresponding monolithic armour. These results were rationalized using published experimental observations pertaining to the effect of MWCNTs on the in-plane and the through-the-thickness properties of fibre-mat/polymer-matrix composite materials.

**Keywords:** vinyl ester epoxy, carbon nanotubes, composite materials, armour

## 1 INTRODUCTION

Recent efforts of the US Army have been aimed at becoming more mobile, deployable, and sustainable while maintaining or surpassing the current levels of lethality and survivability. Current battlefield vehicles have reached in excess of 70 tons due to ever increasing lethality of ballistic threats, which hinders their ability to be readily transported and sustained. Therefore, a number of research and development programs are under way to engineer

light-weight, highly mobile, transportable, and lethal battlefield vehicles with a target weight under 20 tons. To attain these goals, significant advances are needed in the areas of light-weight materials development and multi-functional integration of armour.

The earliest reports of composite light armour developments appear in the late 1960's, when Wilkins and co-workers [1–3] demonstrated the potential of a hybrid armour consisting of a hard ceramic strike face and a thin ductile composite backing. The good ballistic performance of the armour was attributed to the low-density, high hardness, and high compressive strength of the ceramic compound with a high weight-normalized strength and stiffness composite material. The first successful integration of

\*Corresponding author: Department of Mechanical Engineering, Clemson University, 241, Engineering Innovation Building, Clemson, SC 29634, USA. email: mica@ces.clemson.edu

this armour came in the late 1980's where a glass-reinforced polyester hull covered with hard-faced ceramic tiles was developed to replace the aluminum hull of a Bradley Infantry Fighting Vehicle [4]. The resulting vehicle is generally referred to as the Composite Infantry Fighting Vehicle [5]. A composite, ground-up vehicle development program, referred to as the Composite Armoured Vehicle (CAV) program, was subsequently implemented [6]. To meet the stringent weight and ballistic performance requirements of the CAV, the concept of multi-functional polymer-matrix composite-based armour was developed. A schematic of such armour is depicted in Fig. 1.

Each layer in the multi-functional polymer-matrix composite-based armour serves a specific purpose, yet combinations of layers provide role-sharing multi-functionality. A thin, protective polymer-matrix composite face sheet on the outside of the vehicle serves to protect the ceramic-ballistic tiles from incidental damage. The primary role of the ceramic tiles is to break up and/or erode the projectile upon impact. The subsequent rubber-based layer is utilized to improve multi-hit ballistic performance of the armour. The following thick-section composite plate serves as the structural support for the vehicle, a structural backing for the ballistic tiles, and also to assist in catching of the projectile remnants and ceramic-tile fragments and in absorbing their residual kinetic energy. Finally, a fire-protective 'spall' layer of phenolic polymer is incorporated on the inner surface of the vehicle. Other layers can be incorporated to provide additional functionality, such as electro-magnetic ground planes, signature control, etc. [4].

Although the development of the multi-functional armour played an important role in understanding the performance of composite armour, the areal-density normalized ballistic protection performance was found to fall far short of the current requirements.

In the ongoing work [7–10], the potential of next-generation polymer-matrix composites reinforced with carbon nanotubes as advanced light-weight armour is being investigated both computationally and experimentally. It was initially anticipated that,

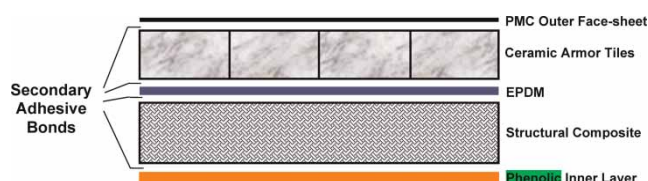


**Fig. 1** A schematic of the multi-functional composite armour

due to a high hardness of the nanotubes, carbon-nanotube reinforced polymer-matrix composite armour may be very effective in eroding/fracturing the projectile while a high strength combined with a high ductility of these composite materials was expected to make them very efficient in absorbing the projectile's kinetic energy.

Before the ballistic performance of such armour could be assessed computationally, a dynamic-material model had to be derived for the nanotube reinforced polymer-matrix composite material. This was done in a series of papers [7–10] using a multi-length scale approach. Specifically: (a) molecular-level computer simulations were used to determine the material mechanical properties of 'effective fibres' (multi-walled carbon nanotubes (MWCNTs) surrounded with a nanometre thick layer of poly-vinyl-ester-epoxy (PVEE) with an altered confirmation) [7]; (b) micro-mechanics type calculations were employed to determine the effective mechanical properties of MWCNT reinforced PVEE composite mats [8]; and (c) continuum level homogenization techniques were used to determine the effective mechanical properties of E-glass reinforced composites with MWCNT-doped PVEE matrix [9]. Once the required material models were derived, a series of transient non-linear dynamics simulations of the impact of a composite armour with a fragment simulating projectile (FSP), were carried out [10] (It should be noted that the term FSP is used to denote a simulated projectile, which mimics a typical fragment generated during explosion of an improvised explosive device (IED). In all of the cases analysed by the present authors, in this work and in prior work, erosion, but not fragmentation of the FSP was observed).

Two distinct architectures of the armour were considered: (a) hybrid armour consisting of a 100- $\mu\text{m}$  thick MWCNT reinforced PVEE-matrix mat sandwiched between two E-glass mat reinforced PVEE-matrix lamina; and (b) a monolithic E-glass reinforced armour in which the PVEE matrix was doped with the same total volume of MWCNTs as in the case of the hybrid armour. The results obtained showed that the use of either of these options gives rise to a relatively small ( $\sim 6$  per cent) increase in the ballistic-protection performance (as quantified by V50, the initial velocity and a given FSP that yields a 50 per cent probability of penetrating the armour) of the composite armour. This finding was rationalized by the fact that, due to the nature of the composite-laminate manufacturing method used, MWCNT reinforcements were aligned parallel to the armour faces. This caused only a minor improvement (less than a per cent) in the through-the-thickness properties.

It was further suggested that the use of MWCNT reinforcements aligned orthogonally to the armour faces ('MWCNT forest') may be more beneficial to

the improvement of the armour's ballistic protection performance. This recommendation was supported by the recent work of Veedu *et al.* [11], reporting substantial (in excess of 100 per cent) increase of composite laminate properties (in particular, the through-the-thickness mechanical properties) in which MWCNTs were aligned in the direction normal to the faces of the composite-laminate.

The objective of the present work is two-fold: (a) to derive and parameterize a material model for MWCNT forest reinforced PVEE matrix mats and (b) to assess the potential of such mats used as armour hard-facing to improve the ballistic protection performance of E-glass mat reinforced PVEE matrix armour. The objective (b) will be addressed in the present work using a series of transient non-linear dynamics computational analyses. In the ongoing work, the objective (b) is also being addressed experimentally. Part of the ongoing work includes fabrication of the MWCNT forest-mat hard-face. These MWCNTs aligned in a perpendicular direction with respect to the substrate (a plain-woven mat of E-glass in the present work) are grown in a tubular furnace using a chemical vapour deposition (CVD) process. The plain-woven E-glass fabric is used as an internal lining of the furnace. A reaction-gas mixture (consisting of a carbon-containing pre-cursor gas, a catalytic-particles pre-cursor gas, and a carrier gas) is fed into the furnace whose (axial) temperature profile is adjusted to yield a uniform deposition rate of MWCNTs along the length of the furnace. The MWCNTs grow orthogonally to the local surface of the furnace inner lining whereas the catalytic particles reside on the top (growing) end of the MWCNTs. This process can yield MWCNT forests with an average MWCNT length of 150–250  $\mu\text{m}$ . Once the MWCNT-forest coated E-glass mat furnace lining is removed and placed on top of the E-glass mats (with the MWCNT-forest side facing outward), a standard vacuum assisted resin transfer moulding (VARTM) process is used to produce the composite armour with a MWCNT-forest hard-face. Upon the completion of fabrication of the hard-faced armour, its ballistic performance is tested by striking armour with cylindrical steel projectiles of differing masses and impact velocities.

The organization of the paper is as follows. A brief overview of the non-linear dynamics computational procedure utilized in the present work is given in section 2.1. Constitutive models used to represent the behaviour of the projectile and the armour materials under ballistic impact conditions are discussed in section 2.2. Details of the numerical model used to analyse the impact and penetration of the armour by a fragment simulating projectile are presented in section 2.3. The results obtained in the present work are presented and discussed in section 3. The main

conclusions resulting from the present work are summarized in section 4.

## 2 COMPUTATIONAL PROCEDURE

### 2.1 Transient non-linear dynamics modelling of projectile/target interactions

Computational assessment of the ballistic-protection performance of armour with respect to IED fragments is generally done by carrying out numerical simulations of the interactions between an FSP and armour (an E-glass mat reinforced PVEE matrix composite laminate hard-faced with a MWCNT-forest-based mat, in the present work). Such calculations have been performed, in the present work, using AUTODYN, a general-purpose transient non-linear dynamics modelling and simulation software [12]. Within AUTODYN, the appropriate mass, momentum and energy conservation equations are combined with the attendant-materials model equations and the appropriate initial and boundary conditions and solved numerically using a second-order accurate explicit scheme. The numerical framework (i.e. the 'processor' as referred to in AUTODYN) used is generally dependent on the physical nature of the problem being studied and, for multi-domain problems, different domains can be analysed using different processors. The Lagrange processor or the SPH (smooth particle hydrodynamics) processor are typically used for solid-continuum structures, whereas the Euler processor is commonly used for modelling gases, liquids, or solids undergoing large deformations and density changes. The Lagrange-based shell and beam processors are designated for modelling shell- and beam-like solid structures, respectively.

In the present work, the ballistic-protection performance of E-glass mat reinforced polymer-matrix composite armours hard-faced with a MWCNT-forest-based mat under FSP threats was analysed using the Lagrange processor. The interactions between the projectile and the armour are accounted for through the use of the sub-domain interaction options within AUTODYN [12], which were over-viewed in detail in our recent work [10]. Also, a detailed discussion regarding the effect of the processor choice (Lagrange versus SPH) for the projectile and the target on the computational results can be found in reference [8].

### 2.2 Material models

The complete formulation of a transient non-linear dynamics problem involving impact of armour by

an FSP entails the knowledge of materials models (material-specific relations between pressure, stress, mass density, strain, strain rate, internal energy density, etc.). These relations typically involve: (a) an equation of state; (b) a strength equation; (c) a failure equation; and (d) an erosion equation for each constituent material. The equation of state defines pressure dependence on mass density and internal-energy density (and, in the case of anisotropic materials, on deviatoric strain). The strength and failure equations define the evolutions of the deviatoric stress in the elastic regime, elastic–plastic regime, and in the post failure initiation regime. In other words, the equation of state along with the strength and failure equations enable assessment of the evolution of the complete stress tensor during a transient non-linear dynamics analysis. Such an assessment is needed where the governing conservation equations are being solved. The erosion equation is generally intended for eliminating numerical solution difficulties arising from highly disordered Lagrangian cells. Nevertheless, the erosion equation is often used to provide additional material failure mechanism especially in materials with limited ductility. When a computational/material cell is eroded, the freed nodes are retained along with their velocities in order to conserve momentum of the system.

In the following two sections, a brief description is given of two material models used in the present work. The first (isotropic) material model is used to represent the behaviour of an AISI 4340-steel FSP. The values of the material parameters for AISI 4340 steel are taken from the AUTODYN materials library [12]. The other (transversely isotropic) material model is used to represent the behaviour of the E-glass mat reinforced MWCNT-doped PVEE composite laminates as well as the MWCNT-reinforced PVEE composite mats (for both the case of MWCNTs aligned parallel with and orthogonal to the mat faces). The corresponding material parameters for the E-glass mat reinforced MWCNT-doped PVEE composite laminates and the MWCNT-reinforced PVEE composite mats with the MWCNTs aligned orthogonal to the mat faces are taken from the previous work [10]. A derivation of the material parameters for the composite material with the MWCNTs aligned normal to the mat faces is carried out in section 3.1 in the present work.

### 2.2.1 AISI 4340 steel

The material model for AISI 4340 steel includes: (a) an (internal-energy density invariant) linear equation of state; (b) a strength modes consisting of the von Mises yield criterion, the Prandtl–Reuss associated flow rule, and the Johnson–Cook flow-strength

model; (c) a stress-based damage-initiation isotropic-softening ductile-failure Johnson–Cook model; and (d) an erosion model based on an instantaneous geometrical strain of 2.0. Since a detailed account of the material model for AISI 4340 steel was given in the recent work [9], no further details of this model will be presented here.

### 2.2.2 Planar isotropic material model for E-glass mat and MWCNT reinforced poly-vinyl-ester epoxy composite laminates

As discussed earlier, the same planar isotropic material model (presented in this section) is used (with different parameterizations) to describe the behaviour of five materials:

- a composite material consisting of a 0.49-vol% MWCNT-doped PVEE matrix, which is reinforced with 53 vol% E-glass mats;
- a composite material consisting of a 0.49-vol% MWCNT-doped PVEE matrix, which is reinforced with 10 vol% MWCNT mats aligned parallel with the armour strike face;
- a composite material consisting of a 0.49-vol% MWCNT-doped PVEE matrix which is reinforced with 30 vol% MWCNT mats aligned parallel with the armour strike face;
- a composite material consisting of a 0.49-vol% MWCNT-doped PVEE matrix, which is reinforced with 10 vol% MWCNT-forest mats;
- a composite material consisting of a 0.49-vol% MWCNT-doped PVEE matrix, which is reinforced with 30 vol% MWCNT-forest mats.

It should be noted that material (a) is used to construct the main body of armour whereas materials (b)–(e) are used (one at a time) as 100- $\mu\text{m}$  thick hard-face. For brevity, the model used to describe mechanical behaviour of the five materials given above (with different parameterizations) will be referred to as the composite-laminate model in the remainder of the manuscript. Before this material model is presented, it should be noted that the materials described are all planar-isotropic with an  $x_2$ – $x_3$  plane of isotropy and the through-the-thickness direction parallel with the  $x_1$ -axis. Also, since a detailed account of this material model was given in the recent work [10], only a brief overview of the key relations will be given in this section.

**2.2.2.1 Equation of state.** A polynomial form of the equation of state is used to represent the pressure dependence on mass density and the internal energy density (i.e. temperature). Furthermore, due to the non-isotropic nature of the material at hand, an additional term is used to represent the pressure dependence of the deviatoric strain

components. Such a term is not present in isotropic materials.

**2.2.2.2 Strength model.** The evolution of the deviatoric part of the stress tensor is described using the planar–isotropic elastic stiffness tensor, a six-parameter parabolic yield function, the Prandtl–Reuss normality flow rule and a piece-wise linear strain hardening constitutive material flow-strength equation. The elastic stiffness tensor is used for deviatoric-stress calculations during elastic loading/unloading and elastic reloading, whereas the yield criterion, the flow rule, and the flow-strength relation are used to update the stress during and elastic–plastic deformation step.

**2.2.2.3 Failure model.** Once the material reaches the condition for damage initiation, the stress evolution is controlled by the progression of damage and not by plastic deformation. The failure model used here utilizes a quadratic stress-based failure initiation criterion (one equation for each of the three principal material planes). Consequently, the failure initiation entails the knowledge of six (three normal and three shear) failure-initiation stresses. Once the failure initiation has occurred on a given principal plane, the material begins to accumulate damage which in turn, causes the quadratic failure surface to shrink. The resulting damage-induced irreversible deformation is also governed by the Prandtl–Reuss normality flow rule. The ultimate failure on a give principle plane takes place when the combined damage arising from the corresponding normal and two shear stress components acquire its maximum allowed value. Such a value is controlled by the corresponding fracture energies. Thus, the damage evolution part of the failure model entails the knowledge of six (three normal and three shear) fracture energies.

**2.2.2.4 Erosion model.** As discussed in the previous work [8], the computational results attained during a transient non-linear dynamics simulation of FSP/armour interactions are quite sensitive to the choice of erosion equation parameters, where the FSP and the armour are both represented using Lagrange models. Consequently, a substantial effort was invested in the previous work in order to arrive at the value of the erosion strain, which ensures that both the ballistic protection (as quantified by V50), and the distribution of the damage as predicted by the model are in good agreement with the experimental counterparts. A strain value of 0.65 was found to be the optimal value for material (a) and 0.70 for materials (b)–(e).

## 2.3 Problem definition and computational analysis

As stated earlier, one of the objectives of the present work is to carry out transient non-linear dynamics analyses of the impact and penetration of E-glass mat reinforced PVEE matrix composite armour hard-faced with a MWCNT-reinforced PVEE-matrix mat by an FSP in order to determine the ballistic-protection performance of such armour. Three distinct armour architectures were considered: (a) a 12.9-mm thick monolithic composite armour based on E-glass reinforced mats and a 0.49-vol% MWCNT-doped PVEE matrix; (b) a hybrid armour based on a 0.2-mm thick 10 or 30 vol% MWCNT-forest reinforced PVEE-matrix hard-face mat and a 12.7-mm thick backing made of the same E-glass reinforced mats and a 0.49-vol% MWCNT-doped PVEE matrix, as in (a); and (c) the same as in (b) but with the MWCNT reinforcements parallel with the armour faces. A summary of the five armour architectures is provided in Tables 1 to 3.

The work was limited to the case of a normal impact of the armour by the FSP and, due to the attendant axi-symmetric nature of the problem, all the calculations were carried out using a two-dimensional (axisymmetric) model. A simple schematic of the projectile/armour impact/penetration problem analysed here is given in Fig. 2. The (0.30 caliber FSP) projectile is cylindrical in shape with a diameter of 7.62 mm and a height of 7.62 mm. The initial normal velocity of FSP was varied in a range between 400 and 500 m/s. A fixed overall thickness of 12.9 mm and a fixed lateral dimension of 80 mm for the armour are used for all the cases analysed.

The Lagrange processor was used to represent both the FSP and the armour. The projectile was analysed using a mesh of 200 rectangular cells and an armour consisting of 540 cells. To improve the accuracy of the analysis, smaller cells were used in the regions of the projectile and the armour involved in the projectile/armour interactions. The interaction between the FSP and the armour was accounted for using the parts coupling option available in AUTODYN [12]. A constant friction coefficient of 0.1 between FSP and armour is used through all the calculations carried out in the present work. Except for the projectile/armour contact surfaces and lateral faces of the armour, (default) zero-stress boundary conditions were prescribed on all faces of the projectile and the armour. To ensure that the blast waves are not reflected at the lateral faces of the armour, the *transmit-type* boundary conditions were applied on the faces. A standard mesh sensitivity analysis was conducted (the results not shown for brevity) in order to ensure that the results obtained were effectively insensitive to variations in the size of the cells used.

**Table 1** Orthotropic equation of state model parameters for materials used in the present work

Parameter	Symbol	Unit	Value				
			MWCNT doped E-glass derakane 510A	MWCNT doped derakane 510A plus in-plane MWCNT mat		MWCNT doped derakane 510A plus MWCNT forest mat	
				10%	30%	10%	30%
Density	$\rho$	g/cm <sup>3</sup>	1.9349	1.23	1.23	1.23	1.23
Young's modulus 11	$E_{11}$	kPa	$2.0899 \times 10^7$	$3.2320 \times 10^7$	$6.1126 \times 10^6$	$6.1126 \times 10^6$	$8.7189 \times 10^7$
Young's modulus 22	$E_{22}$	kPa	$4.3046 \times 10^7$	$4.6053 \times 10^6$	$1.3806 \times 10^7$	$1.3806 \times 10^7$	$5.9408 \times 10^6$
Young's modulus 33	$E_{33}$	kPa	$4.3046 \times 10^7$	$4.6053 \times 10^6$	$1.3806 \times 10^7$	$1.3806 \times 10^7$	$5.9408 \times 10^6$
Poisson's ratio 12	$V_{12}$	–	0.1751	0.353 714	0.174 786	0.174 786	0.293 245
Poisson's ratio 23	$V_{23}$	–	0.1080	0.598 707	0.342 873	0.342 873	0.293 245
Poisson's ratio 31	$V_{31}$	–	0.3608	0.050 402	0.394 793	0.394 793	0.019 981
Shear modulus 12	$G_{12}$	kPa	$6.0290 \times 10^6$	$1.3776 \times 10^6$	$1.4086 \times 10^6$	$1.4086 \times 10^6$	$1.7500 \times 10^6$
Shear modulus 23	$G_{23}$	kPa	$6.7433 \times 10^6$	$1.4404 \times 10^6$	$3.1847 \times 10^6$	$3.1847 \times 10^6$	$2.2000 \times 10^6$
Shear modulus 31	$G_{31}$	kPa	$6.0290 \times 10^6$	$1.3776 \times 10^6$	$1.4086 \times 10^6$	$1.4086 \times 10^6$	$1.7500 \times 10^6$
Bulk modulus	$K$	kPa	$1.9579 \times 10^7$	$8.7204 \times 10^6$	$8.8361 \times 10^7$	$8.8361 \times 10^7$	$1.5762 \times 10^7$
Volumetric parameter	$A_2$	kPa	$5.0000 \times 10^7$	$5.0000 \times 10^7$	$5.0000 \times 10^7$	$5.0000 \times 10^7$	$5.0000 \times 10^7$
Volumetric parameter	$A_3$	kPa	0	0	0	0	0
Volumetric parameter	$B_0$	kPa	0	0	0	0	0
Volumetric parameter	$B_1$	kPa	0	0	0	0	0
Specific heat	$C_v$	J/kgK	$1.4200 \times 10^3$	$1.4200 \times 10^3$	$1.4200 \times 10^3$	$1.4200 \times 10^3$	$1.4200 \times 10^3$
Reference temperature	$T_{ref}$	K	300	300	300	300	300

**Table 2** Orthotropic yield strength model parameters for materials used in the present work

Parameter	Symbol	Unit	Value				
			MWCNT doped E-glass derakane 510A	MWCNT doped derakane 510A plus in-plane MWCNT mat		MWCNT doped derakane 510A plus MWCNT forest mat	
				10%	30%	10%	30%
Stress parameter 11	$A_{11}$	–	40.5730	0.1038	1.1107	1.1107	0.0200
Stress parameter 22	$A_{22}$	–	1.0000	1.0000	1.0000	1.0000	1.0000
Stress parameter 33	$A_{33}$	–	1.0000	1.0000	1.0000	1.0000	1.0000
Stress parameter 12	$A_{12}$	–	–8.1789	–0.3646	–0.5395	–0.5395	–0.4522
Stress parameter 23	$A_{23}$	–	–8.1789	–0.3646	–0.5395	–0.5395	–0.4522
Stress parameter 31	$A_{31}$	–	–0.5000	–0.5000	–0.5000	–0.5000	–0.5000
Stress parameter 44	$G_{12}$	–	1.5000	1.5000	1.5000	1.5000	1.5000
Stress parameter 55	$G_{23}$	–	28.9650	0.916 570	1.5950	1.5950	0.9622
Stress parameter 66	$G_{31}$	–	28.9650	0.916 570	1.5950	1.5950	0.9622
Effective stress	$\sigma_{eff}$	kPa	$7.7434 \times 10^5$	$6.4924 \times 10^4$	$8.8678 \times 10^4$	$8.8678 \times 10^4$	$1.6754 \times 10^6$

**Table 3** Orthotropic softening failure model parameters for materials used in the present work

Parameter	Symbol	Unit	Value				
			MWCNT doped E-glass derakane 510	MWCNT doped derakane 510A plus in-plane MWCNT mat		MWCNT doped derakane 510A plus MWCNT forest mat	
				10%	30%	10%	30%
Failure stress	$\sigma_{11}$	kPa	$1.19110 \times 10^5$	$8.2441 \times 10^4$	$9.7734 \times 10^4$	$1.7271 \times 10^5$	$8.0893 \times 10^5$
Failure stress	$\sigma_{22}$	kPa	$6.5121 \times 10^5$	$8.6886 \times 10^4$	$1.1674 \times 10^5$	$6.3612 \times 10^4$	$2.2618 \times 10^5$
Failure stress	$\sigma_{33}$	kPa	$6.5121 \times 10^5$	$8.6886 \times 10^4$	$1.1674 \times 10^5$	$6.3612 \times 10^4$	$2.2618 \times 10^5$
Failure stress	$\sigma_{12}$	kPa	$9.9680 \times 10^4$	$4.8648 \times 10^4$	$6.0431 \times 10^4$	$4.6983 \times 10^4$	$1.8770 \times 10^5$
Failure stress	$\sigma_{23}$	kPa	$3.7598 \times 10^5$	$5.0164 \times 10^4$	$6.7400 \times 10^4$	$3.6727 \times 10^4$	$1.6821 \times 10^5$
Failure stress	$\sigma_{31}$	kPa	$9.9680 \times 10^4$	$4.8648 \times 10^4$	$6.0431 \times 10^4$	$4.6983 \times 10^4$	$1.8770 \times 10^5$
Fracture energy	$G_{11}$	J/m <sup>2</sup>	744	927	1100	864	2045
Fracture energy	$G_{22}$	J/m <sup>2</sup>	326	1086	1459	716	745
Fracture energy	$G_{33}$	J/m <sup>2</sup>	326	1086	1459	716	745
Fracture energy	$G_{12}$	J/m <sup>2</sup>	1246	730	906	705	716
Fracture energy	$G_{23}$	J/m <sup>2</sup>	846	752	1011	551	573
Fracture energy	$G_{31}$	J/m <sup>2</sup>	1246	730	906	705	716
Erosion strain	$\epsilon$	–	0.65	0.70	0.70	0.70	0.70

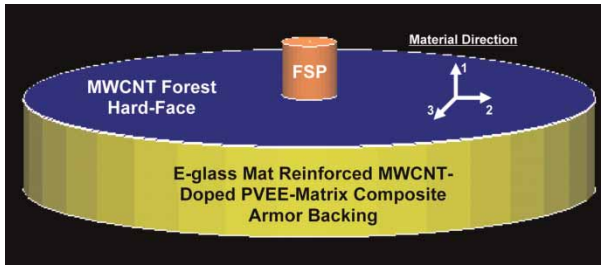


**Fig. 2** An example of the computational domain used in the present work to analyse the interactions between a FSP and composite armour hard-faced with a MWCNT-forest mat

### 3 RESULTS AND DISCUSSION

#### 3.1 Material model for MWCNT-forest reinforced PVEE matrix mats

As discussed earlier, the material model for E-glass mat-reinforced MWCNT-doped PVEE-matrix composite and for the MWCNT-reinforced PVEE-matrix mats (in which the MWCNT reinforced mats are aligned parallel with the mat faces) were determined in reference [10]. In this section, a brief description is given of the procedure used to determine the material model for MWCNT-forest reinforced PVEE-matrix mats. Before this procedure is presented, however, a brief description is given of the process, which is being utilized in the ongoing work to process such mats.

#### 3.2 Derivation of material model for MWCNT-forest reinforced PVEE-matrix composite mats

In this section, an attempt is made to derive a simple material model for the MWCNT-forest reinforced PVEE-matrix composite mats. The model developed in the section is based on three assumptions: (a) the in-plane composite-material properties are controlled by the PVEE-matrix; (b) the through-the-thickness composite material properties are controlled by the MWCNT-forest; and (c) the effect of the interactions between the PVEE matrix with the MWCNT forest can be accounted for using the recently developed planar-isotropic material model for the MWCNT-reinforced PVEE-matrix composite [7–8]. A summary of the material model parameters for the equation of state, strength model, failure model, and the erosion model for (10 and 30 vol%) MWCNT-forest reinforced PVEE-matrix composite mats obtained in the present work are given in Tables 1 to 3, respectively. It should be noted that within the coordinate system chosen in the present

work, the through-the-mat-thickness direction coincides with the  $x_1$ -axis.

It should be observed that Tables 1 to 3 contain a large number of parameters. These parameters were obtained in the previous work [7, 8] by conducting molecular-level mechanical-test analyses with micromechanics homogenization procedures. The results of these procedures were then fitted using the composite laminate material model [12], which contains the equations of state parameters ( $A_2, A_3, B_0, B_1$ ), strength parameters ( $A_{11}$  to  $A_{31}, G_{12}, G_{23}, G_{31}$ ), and failure parameters ( $\sigma_{11}$  to  $\sigma_{31}, G_{11}$  to  $G_{13}$ ). A complete experimental validation of the material model was not carried out, but the results for V50 and the extent of surrounding damage observed in ballistic tests were, in the case of in-plane MWCNT-mats reinforced PVEE-matrix composite, predicted by the model.

It should also be noted that no direct experimental validation of the material model was carried out in the present work. The sponsor of this project was interested in a physics-based model (obtained by modifying an existing model for polymer-matrix laminates), which can provide reasonable predictions of V50 and the extent of surrounding damage in the armour. The ongoing experimental work [13] has yielded preliminary results, which suggest that the model developed here provides a reasonable prediction of armour ballistic-impact conditions.

##### 3.2.1 Equation of state

Due to the planar-isotropic nature of the material at hand, an orthotropic material model (with interchangeability of the  $x_2$  and  $x_3$  direction related properties) is developed. Within this model the pressure,  $P$ , dependence on the compaction,  $\mu = (\rho/\rho_0 - 1)$ , (where  $\rho$  is density and  $\rho_0$  initial density) and temperature,  $T$ , is defined as

$$P = -K\mu + A_2\mu^2 - A_3\mu^3 + (B_0 - B_1\mu)\rho_0 e - \frac{1}{3}(C_{11} + 2C_{12})e_{11}^d - \frac{1}{3}(C_{12} + C_{22} + C_{23})(e_{22}^d + e_{33}^d) \quad (1)$$

where  $K$  is the bulk modulus defined as

$$K = \frac{1}{9}[C_{11} + 2C_{22} + 4C_{12} + 2C_{23}] \quad (2)$$

where  $e = C_v(T - T_{\text{ref}})$  is the internal energy density,  $C_v$  is the material specific heat,  $T_{\text{ref}}$  is an inertial energy-density reference temperature,  $C_{ij}$ 's are the material stiffness coefficients (coefficients of the material  $6 \times 6$  stiffness matrix),  $e_{ij}^d$ 's are the components of the deviatoric strain matrix, and  $A_2, A_3,$

$B_0, B_1$  are material-specific parameters. The last term on the right-hand side of equation (1) represents the coupling between pressure and the deviatoric strain and is absent in isotropic materials.

Equation (1) shows that a complete definition of the equation of state entails the knowledge of the planar-isotropic elastic-constants of the material ( $C_{11}, C_{22}, C_{12}, C_{23}, C_{44}$ , and  $C_{55}$ ) as well as the specification of  $A_2, A_3, B_0, B_1, C_v$ , and  $T_{ref}$ . It should be noted that only normal deviatoric strain components appear in the pressure-deviatoric strain coupling term. This is not an approximation but a direct result of a simple derivation of the pressure-deviatoric strain coupling [12].

The aforementioned elements of the elastic stiffness matrix were determined using the micromechanics-based Mori–Tanka type elastic homogeneity model developed in the previous work [8].

Due to the similarity in the chemical make-up and microstructure between the MWCNT-forest mats and the ones in which the MWCNT reinforcements are parallel with the mat faces (the model for the latter material was derived in the previous work [10]), the values for  $A_2, A_3, B_0, B_1, C_v$ , and  $T_{ref}$  are set equal in the two materials.

### 3.2.2 Strength model

The strength model is defined as a combination of the yield criterion, the plastic-flow rule and the constitutive material model. To account for the planar-isotropic nature of the material at hand, a six-parameter parabolic yield-function (criterion) is used which can be written as

$$f(\sigma_{ij}) = a_{11}\sigma_{11}^2 + a_{22}(\sigma_{22}^2 + \sigma_{33}^2) + 2a_{12}\sigma_{11}(\sigma_{22} + \sigma_{33}) + 2a_{23}\sigma_{22}\sigma_{33} + 2a_{44}\sigma_{23}^2 + 2a_{55}(\sigma_{31}^2 + \sigma_{12}^2) - k \leq 0 \quad (3)$$

Among the seven material-specific parameters  $a_{11}$ – $a_{66}$  and  $k$ , one can be set independently. In the present work,  $a_{22}$  is set to 1. It should be noted that only nine out of ten parameters appearing in equation (3) are independent, hence one of these parameters can be set independently without any effect on the computational results.

The values of the remaining parameters in equation (5) are defined using the yield stress values corresponding to the  $x_1, x_2$  ( $\sigma_{11,y}$  and  $\sigma_{22,y}$ , respectively,) and balanced-biaxial  $x_1$ – $x_2$  yield stress ( $\sigma_{12,y, bal\_biaxial}$ )

$$k = \sigma_{22,y}^2 \quad (4)$$

$$a_{11} = \frac{\sigma_{22,y}^2}{\sigma_{11,y}^2} \quad (5)$$

$$a_{12} = \left( \frac{k}{\sigma_{12,y, bal\_biaxial}^2} - a_{11} - a_{22} \right) \left( \frac{1}{2} \right) \quad (6)$$

$$a_{23} = -0.5a_{22} \quad (7)$$

$$a_{44} = \frac{3}{2}a_{22} \quad (8)$$

$$a_{55} = (a_{11} - a_{22} - 2a_{12}) \left( \frac{1}{2} \right) \quad (9)$$

It should be noted that some of the relations between different  $a_{ij}$ 's (e.g. equation (6)) were obtained from the recognition of the material isotropy in the  $x_2$ – $x_3$  plane. Consequently, the corresponding relations in the isotropic materials were used.

The direction of the plastic flow is defined using the Prandtl–Reuss normality flow rule. As far as the constitutive equation (the equation, which defines the rate at which material flow-strength increases as the equivalent plastic strain increases) is concerned, a piece-wise linear form is used. It should be noted that an analogous procedure for the derivation of a material model for the PVEE matrix composite material reinforced with MWCNTs aligned parallel with the mat faces was used in the recent work [10], where additional details for the procedure can be found.

### 3.2.3 Failure model

A stress-based failure initiation criterion is combined with orthotropic softening (ductile failure) to find the material failure model. A complete definition of this model entails the knowledge of six (three normal and three shear) failure initiation stresses and six corresponding fracture energies. However, due to the planar-isotropic nature of the material at hand, only four (unique) failure initiation stresses and four fracture energies were needed. The values for these quantities were determined previously in the multi-length scale computational analysis of the material at hand [10].

### 3.2.4 Erosion

To prevent run-time errors from occurring as a result of highly distorted Lagrangian cells, an erosion model is also defined for the material at hand. To ensure that a constant erosion criterion is defined for all the materials used in the present work, erosion is set to

occur when the instantaneous geometric (elastic + plastic + crack) strain reaches a value of 0.65.

It should be noted that some of the parameters (e.g.  $A_2$ ,  $A_3$ ,  $B_0$ ,  $B_1$ ) were left independent of the orientation of MWCNT mat orientation (forest versus ply). This was done because the terms in question had a secondary effect on the computational results, as confirmed in the previous work [10]. Since  $B_0$  and  $B_1$  were set to 0.0, the values of  $C_v$  and  $T_{ref}$  are hence immaterial. Conversely, model parameters, which have a first-order effect (e.g. failure strengths and fracture energies, Table 3) were assessed and they are significantly different for the forest and in-plane MWCNT mats.

### 3.3 Armour hard-facing with MWCNT-reinforced PVEE-matrix composite mats

In this section, the potential benefits of hard facing the E-glass fibre-mat reinforced armour with MWCNT-reinforced PVEE-matrix composite mats is explored. Toward that end, a monolithic E-glass/PVEE-matrix armour with a thickness of 12.9 mm is selected as the 'control'. The PVEE-matrix in this armour is doped with a 0.5-vol% of MWCNTs, following the recommendation made in the prior work [10] with regard to the benefits of doping the PVEE matrix with the MWCNTs. The ballistic-protection performance of the control with respect to a 30 caliber FSP has been assessed by impacting the armour with the FSP. The FSP's initial velocity is varied in a range between 400 and 425 m/s.

The results of this calculation are displayed in Figs 3(a) and (b). The results displayed in Fig. 3(a) suggest that the initial velocity of the projectile, which ensures armour penetration with a minimal residual velocity is within the range of 405–415 m/s. It should be noted that the results displayed in Fig. 3(a) and its subsequent counterparts are given for a minimal time period required to attain a constant residual velocity of the projectile in each case. While all of the calculations carried out in the present work are of a deterministic nature, this velocity will be referred to in the remainder of the manuscript as V50 velocity (the initial velocity at which the probability for armour penetration by the projectile is ~50 per cent). Note that a negative value of the terminal velocity indicates that the FSP has been fully defeated by the armour and it is forced to bounce back. A material deformation/failure plot for the control after impact with an FSP (initially propelled at a velocity of 415 m/s) is displayed in Fig. 3(b). Regions associated with different dominant deformation/failure modes are indicated. The results displayed in Fig. 3(b), as well as the results displayed in Figs 4(b), 5(b), 6(b), and 7(b) show no evidence of

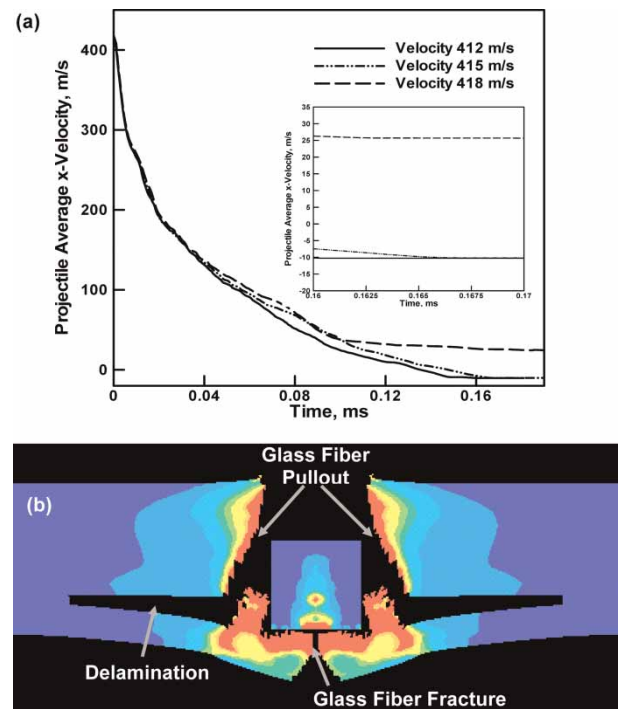


**Fig. 3** (a) Temporal evolution of a 0.30 caliber FSP velocity during impact with a 12.9-mm thick monolithic E-glass continuous fibre-reinforced MWCNT-doped poly-vinyl-ester-epoxy matrix composite armour and (b) deformation/damage distribution for the case of the FSP's initial velocity of 415 m/s

FSP erosion despite the fact that an erosion strain of 0.65 for this material was used in the calculations. This value for the FSP was obtained in the previous work [13] in which the interactions between an FSP and ceramic-hard-faced armour was analysed.

Next, the effect of hard-facing the monolithic armour, discussed above, with a 0.2-mm thick PVEE-matrix mat reinforced with 10 or 30 vol% MWCNTs aligned in a direction parallel to the armour faces are given. The results of the ballistic performance analysis of the resulting hybrid armour are shown in Figs 4(a) and (b) and 5(a) and (b) for the cases of 10 and 30 vol% MWCNTs, respectively. The results displayed in these figures indicate that the presence of the 0.2-mm thick PVEE-matrix mat reinforced with either 10 or 30 vol% MWCNTs aligned in a direction parallel to the armour faces does not noticeably affect either the V50 (remains within the range of 405–415 m/s) or the distribution of the impact induced damage in the armour.

Finally, the effect of hard-facing the monolithic armour, discussed above, with a 0.2-mm-thick PVEE-matrix mat reinforced with 10 or 30 vol% MWCNTs aligned orthogonal to the armour faces (MWCNT forest). The results of the ballistic performance

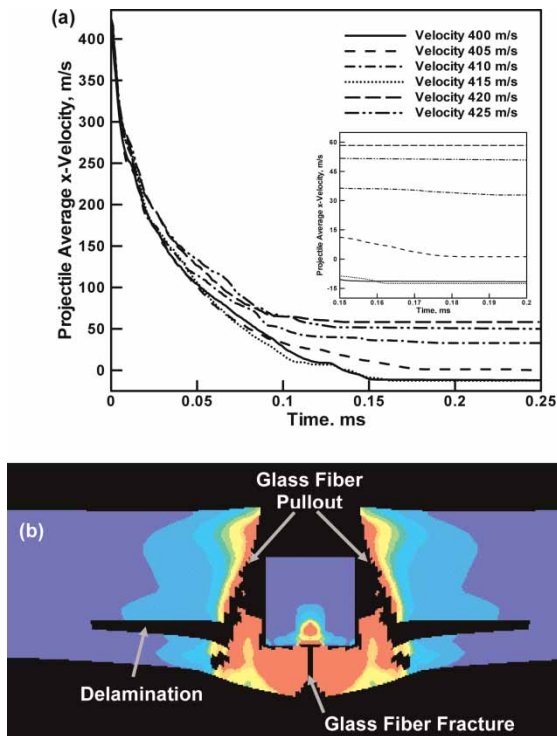


**Fig. 4** (a) Temporal evolution of a 0.30 caliber FSP velocity during impact with a 12.9-mm thick hybrid armour E-glass continuous fibre-reinforced MWCNT-doped PVEE matrix composite hard-faced with a 0.2-mm thick 10 vol% MWCNT ply mat and (b) deformation/damage distribution for the case of the FSP's initial velocity of 415 m/s

analysis of the resulting hybrid armour are shown in Figs 6(a) and (b) and 7(a) and (b) for the cases of 10 and 30 vol% MWCNTs, respectively. The results displayed in these figures indicate that the presence of the 0.2-mm thick PVEE-matrix mat reinforced with 10 vol% MWCNT forests does not noticeably affect either the V50 (remains within the range of 405–415 m/s) or the distribution of the impact induced damage in the armour. Conversely, in the case of 30 vol% MWCNT forest mats, a noticeable but minor (5–10 m/s) increase in the V50 is observed, Fig. 7(a), whereas no significant changes to the distribution of impact induced damage in the armour can be detected, Fig. 7(b). It should be noted that the results shown in Fig. 7(b) correspond to a post impact time that which is a few per cent longer than that corresponding to Fig. 5(b), which accounts for the fact that the extent of damage in the armour is somewhat higher in Fig. 7(b).

The observed improvement in the ballistic performance of the E-glass/doped-PVEE-matrix composite armour hard-faced with a layer of MWCNT-forest mats is consistent with the observation made by Cao *et al.* [14] that, in a MWCNT-forest mat, it is difficult

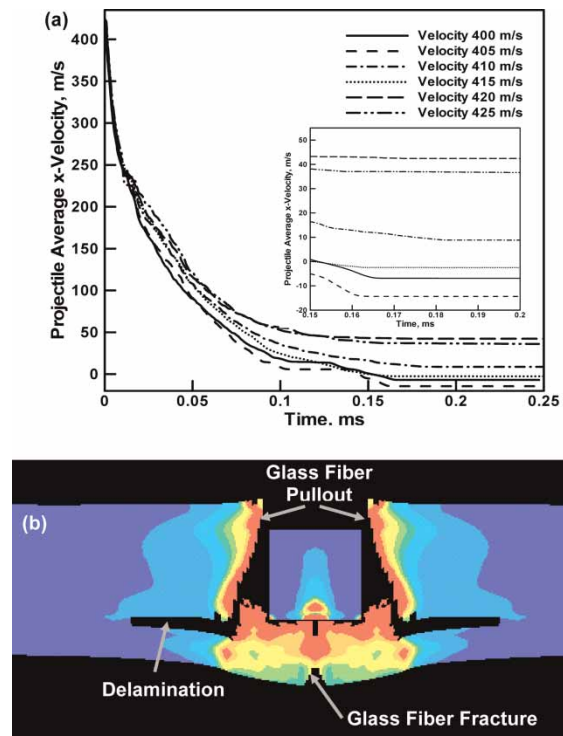


**Fig. 5** (a) Temporal evolution of a 0.30 caliber FSP velocity during impact with a 12.9-mm thick hybrid armour E-glass continuous fibre-reinforced MWCNT-doped PVEE matrix composite hard-faced with a 0.2-mm thick 30 vol% MWCNT ply mat and (b) deformation/damage distribution for the case of the FSP's initial velocity of 415 m/s

for nanotubes to buckle independently because of the proximity of the neighboring tubes. The cooperative nature of the buckling results in a self-organized, zigzag-folded morphology, which is the most space-efficient and energetically favourable configuration for huge numbers of nanotubes to adopt under large compressive strains brought about by the FSP. The folding associated with this zigzag buckling does not require any extra space to accommodate the vertical deformations and acts as a very efficient mechanism for absorption of the kinetic energy carried out by the FSP. In addition, the upright orientation of the nanotubes allows them to make direct contact with the FSP promoting its erosion. Unfortunately, the extent of ballistic protection improvement brought about by the use of 30 vol% MWCNT forest mats as armour hard-facing observed in the present work is only about 1–2 per cent. This finding is not completely unexpected considering the fact that: (a) the hard-facing represents roughly only 1/65th of the armour thickness and (b) due to high compliance of the armour in the through-the-thickness direction and low in-plane strength of the MWCNT mats, the FSP impact was found to cause compressive

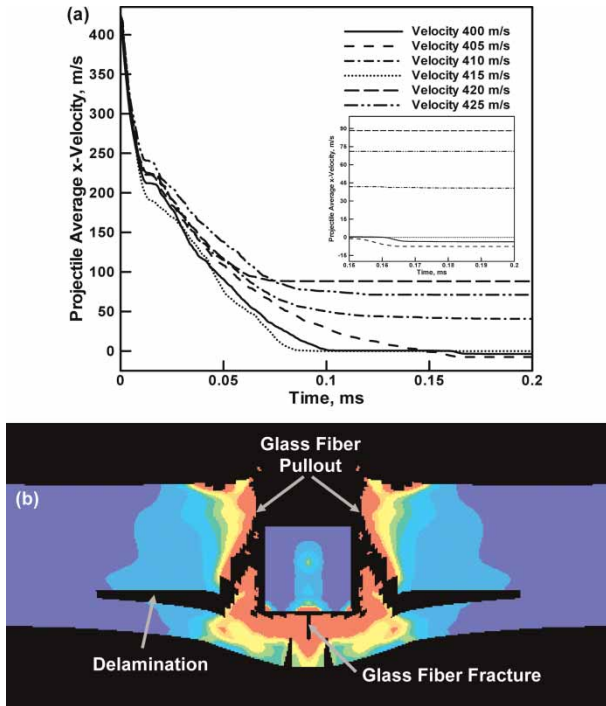


**Fig. 6** (a) Temporal evolution of a 0.30 caliber FSP velocity during impact with a 12.9-mm thick hybrid armour E-glass continuous fibre-reinforced MWCNT-doped PVEE matrix composite hard-faced with a 0.2-mm thick 10 vol% MWCNT forest mat and (b) deformation/damage distribution for the case of the FSP's initial velocity of 415 m/s

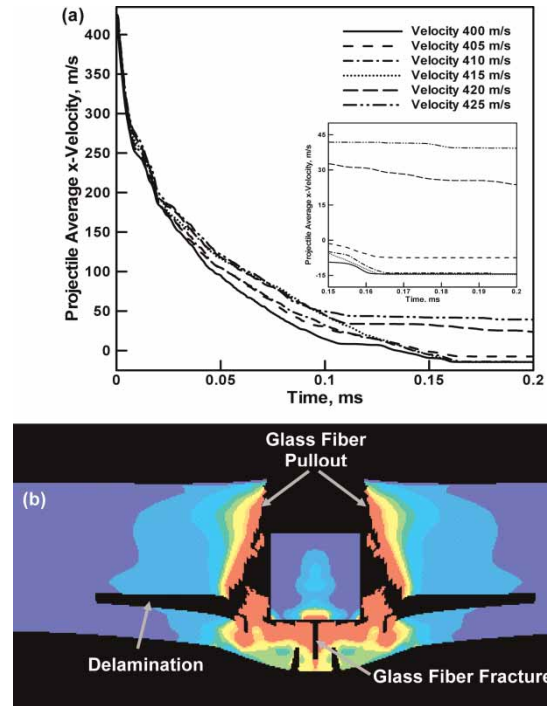


**Fig. 7** (a) Temporal evolution of a 0.30 caliber FSP velocity during impact with a 12.9-mm thick hybrid armour E-glass continuous fibre-reinforced MWCNT-doped PVEE matrix composite hard-faced with a 0.2-mm thick 30 vol% MWCNT forest mat and (b) deformation/damage distribution for the case of the FSP's initial velocity of 415 m/s

deformation predominately in the E-glass PVEE matrix composite. This allowed a circular hole of the size of the FSP to be punched-out in the MWCNT forest mat without considerable mat compression. In other words, due to the compliant nature of the bulk section of the armour, the full potential of the MWCNT forest mats was not utilized. The shortcomings of the current architecture of the E-glass PVEE matrix composite armour hard-faced with MWCNT forest mats can be overcome by: (a) the use of multiple layers of these MWCNT forest mats throughout the full thickness of the bulk section of the armour; (b) depositing MWCNT forests onto ceramic tiles and using such tiles for hard-facing as in the case of the multi-functional composite armour depicted in Fig. 1. In addition, following the observations of Veedu *et al.* [11] that interlacing of fibre-mat/polymer matrix composites with MWCNT forest mats increases tensile transverse properties, the delamination resistance of the armour can be perhaps improved by placing dual-sided MWCNT forest mats closer to the back/spall face of the armour where significant delamination typically occurs.

The results obtained in the present work reveal that despite the fact that all the calculations were of a deterministic nature, generally no single valued V50 is found. This is clearly seen in Fig. 8 in which the terminal FSP's velocity is plotted as a function of the projectile's initial velocity. The results displayed in this figure clearly demonstrate that there is a range of initial FSP velocity in which the projectile may or may not penetrate the armour depending on the exact value of its initial velocity. This finding demonstrates the full complexity of the projectile/armour interaction accompanied by plastic deformation, failure, and erosion of the participating materials. The oscillations in the terminal velocity observed in Fig. 8 cannot be readily explained. Nevertheless, the most logical explanation is that the interactions between the freed nodes (produced after erosion of the Lagrangian elements) leads to a complex multi-body system, which can result in different terminal velocity of the FSP.

Similar oscillatory variations of the FSP projectile velocity with a change in the initial FSP velocity have been previously observed in ceramic-hard-faced light composite armour [13]. Hence, this observation

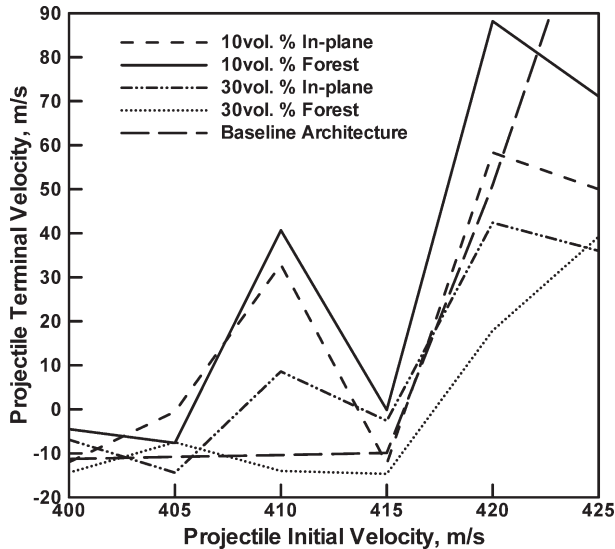


**Fig. 8** Variation of the projectile's terminal velocity as a function of its initial velocity. Negative values of the terminal velocity denote the defeat of the project by the armour

cannot be readily characterized as a deficiency of the present material model or the computational procedure. Rather, this observation reflects the complex nature of the FSP/armour interactions where the extent and the distribution of damage in armour regions surrounding the FSP, and not only the region below the projectile, affect the outcome of an FSP/armour interaction. Furthermore, similar uncertainties in determining V50 experimentally are generally encountered.

Considering the fact that the uncertainty in the determination of V50 is comparable with the highest observed increase in this quantity with changes in armour architecture, one must be careful about claiming that the use of MWCNT forest strike face can indeed lead to improvements in the ballistic performance of light composite armour. This point has been partly confirmed in the ongoing experimental investigations [15] of the E-glass mat reinforced PVEE-matrix armour hard-faced with ca. 17 per cent in-plane MWCNT-reinforced PVEE-matrix composite. Preliminary results showed no statistically significant improvement in V50 relative to the same armour without hard-facing.

#### 4 SUMMARY AND CONCLUSIONS

Based on the results obtained in the present work, the following summary and main conclusions can be made.

1. A simple micro-mechanics model for the material elastic properties and a lower-bound estimate for

the strength and failure properties are used to construct a ballistic material model for MWCNT forest mats (mats in which MWCNTs are aligned orthogonal to the mat faces) containing a poly-vinyl-ester-epoxy matrix.

2. A series of transient non-linear dynamics analyses of the impact of E-glass/PVEE-matrix composite armour hard-faced with a MWCNT-forest mat with a fragment simulating projectile is carried out. The results obtained showed that at 10 vol% of MWCNTs in the hard-face mat, no measurable improvement is obtained. At 30 vol% of MWCNTs, a 1–2 per cent gain in the ballistic protection performance of the armour is observed. Although this enhancement is somewhat questionable considering the fact that significant uncertainty exists relative to the determination of V50, it appears that the observed lack in ballistic resistance improvement is related to inferior in-plane strength properties of the composite laminate armour.
3. Since, similar improvements in the armour penetration resistance were not obtained in the case of armour hard-facing with the mats containing 30 vol% of MWCNTs, but with the MWCNTs lying parallel with the armour faces, the present work revealed that the mode of nanotube deformation plays an important role in the effectiveness of MWCNT-based mats as armour hard-facing.
4. Potential directions for obtaining significant improvements in the ballistic protection performance of the armour through the use of MWCNT mats are identified and discussed.
5. The computational approach presented in the present work showed that transient non-linear dynamics simulations of the projectile/armour interactions can provide critical insight into that deformation and fracture mechanisms controlling the ballistic performance of armour. In addition, the computational procedure reveals stochastic effects of the projectile/armour interactions which are commonly observed experimentally, and usually attributed to variability in armour architecture and material properties.

#### ACKNOWLEDGEMENTS

The material presented in the current paper is based on work supported by the Naval Research Office under the Grant Number N00014-05-1-0844, by the US Army/Clemson University Cooperative Agreements Number W911NF-04-2-0024 and by the US Army Grant Number DAAD19-01-1-0661. The authors are indebted to Dr Tom Juska of the Naval Research Laboratory and to Dr Walter Roy and Dr Fred Stanton from the Army Research Laboratory.

## REFERENCES

- 1 **Wilkins, M. L.** Second progress report of the light armor program. Technical report no. UCRL 50284, Lawrence Livermore National Laboratory, Livermore, CA, 1967.
- 2 **Wilkins, M. L.** Third progress report of the light armor program. Technical report no. UCRL 50349, Lawrence Livermore National Laboratory, Livermore, CA, 1968.
- 3 **Wilkins, M. L., Cline, C. F., and Honodel, C. A.** Fourth progress report of the light armor program. Technical report no. 50694, Lawrence Livermore National Laboratory, Livermore, CA, 1969.
- 4 **Cheesman, B. A., Jensen, R., and Hopped, C.** Protecting the future force: advanced materials and analysis enable robust composite armor. *AMPTIAC Q.*, 2005, **8**, 37.
- 5 **Thomas, G., Larson, A., and Garces, J.** Composite hull program final technical report. Army Research Laboratory Contractor Report No. ARL-CR-179, 1994.
- 6 **Pike, T., McArthur, M., and Schade, D.** Vacuum-assisted resin transfer molding of a layered structural laminate for application on ground combat vehicles. In Proceedings of the 28th International SAMPE Technical Conference, Seattle, WA, 4–7 November 1996, pp. 374–380.
- 7 **Grujicic, M., Sun, Y.-P., and Koudela, K. L.** The effect of covalent functionalization of carbon nanotube reinforcements on the atomic-level mechanical properties of poly-vinyl-ester-epoxy. *Appl. Surf. Sci.*, 2007, **253**, 3009.
- 8 **Grujicic, M., Sun, Y.-P., and Koudela, K. L.** Micro-mechanics based derivation of the materials constitutive relations for carbon nanotube reinforced poly-vinyl-ester-epoxy based composites. *J. Mater. Sci.*, 2007, **42** (12), 4609–4623.
- 9 **Grujicic, M., Pandurangan, B., Angstadt, C. D., Koudela, K. L., and Cheeseman, B. A.** Ballistic-performance optimization of a hybrid carbon-nanotube/E-glass reinforced poly-vinyl-ester-epoxy-matrix composite armor. *J. Mater. Sci.*, 2007, **42**, 5347–5349.
- 10 **Grujicic, M., Bell, W. C., Koudela, K. L., and Cheeseman, B. A.** Ballistic-protection performance of carbon-nanotube doped poly-vinyl-ester-epoxy matrix composite armor reinforced with E-glass fiber mats. *Mater. Sci. Eng. A*, 2007, accepted for publication.
- 11 **Veedu, V. P., Cao, A., Li, X., Ma, K., Soldano, C., Kar, S., Ajayan, P. M., and Ghasemi-Nejhad, M. N.** Multifunctional composites using reinforced laminae with carbon-nanotube forests. *Nat. Mater.*, 2006, **5**, 457.
- 12 **AUTODYN-2D and 3D.** *User documentation*, version 6.1, Century Dynamics Inc., 2006.
- 13 **Grujicic, M., Pandurangan, B., Angstadt, C. D., Zecevic, U., Koudela, K. L., and Cheeseman, B. A.** Ballistic performance of alumina/S-2 glass fiber-reinforced polymer-matrix composite hybrid lightweight armor against armor piercing (AP) and non-AP projectiles. *Multidis. Model. Mater. Struct.*, 2007, **3**, 1–15.
- 14 **Cao, A., Dickrell, P. L., Sawyer, W. G., Ghasemi-Nejhad, M. N., and Ajayan, P. M.** Super-Compressible foamlike carbon nanotube films. *Science*, 2005, **310**, 1307.
- 15 **Koudela, K. L.** Work in progress. Pennsylvania State University Applied Research Laboratory, May 2007.